9-16-2014

Calculating the Velocity of a Fast-Moving Snow Avalanche Using an Infrasound Array

Scott Havens
Boise State University

Hans-Peter Marshall
Boise State University

Jeffrey B. Johnson
Boise State University

Bill Nicholson
Idaho Transportation Department

AGU PUBLICATIONS

Geophysical Research Letters

RESEARCH LETTER
10.1002/2014GL061254

Key Points:
- Avalanche velocity time series with uncertainty estimated from infrasound
- Possible detection of initial snow pack failure prior to the avalanche
- Provide new insight into flow dynamics for a mass wasting event

Correspondence to:
S. Havens,
scotthavens@boisestate.edu

Citation:
Havens, S., H.-P. Marshall, J. B. Johnson, and B. Nicholson (2014), Calculating the velocity of a fast-moving snow avalanche using an infrasound array, *Geophys. Res. Lett.*, *41*, 6191–6198, doi:10.1002/2014GL061254.

Received 18 JUL 2014
Accepted 22 AUG 2014
Accepted article online 26 AUG 2014
Published online 8 SEP 2014

Calculating the velocity of a fast-moving snow avalanche using an infrasound array

Scott Havens[1], Hans-Peter Marshall[1], Jeffrey B. Johnson[1], and Bill Nicholson[2]

[1]Center for Geophysical Investigation of the Shallow Subsurface, Boise State University, Boise, Idaho, USA, [2]Idaho Transportation Department, Boise, Idaho, USA

Abstract On 19 January 2012, a large D3 avalanche (approximately 10^3 t) was recorded with an infrasound array ideally situated for observing the avalanche velocity. The avalanche crossed Highway 21 in Central Idaho during the largest avalanche cycle in the 15 years of recorded history and deposited approximately 8 m of snow on the roadway. Possible source locations along the avalanche path were estimated at 0.5 s intervals and were used to calculate the avalanche velocity during the 64 s event. Approximately 10 s prior to the main avalanche signal, a small infrasound signal originated from the direction of the start zone. We infer this to be the initial snow pack failure, a precursory signal to the impending avalanche. The avalanche accelerated to a maximum velocity of 35.9 $\pm$ 7.6 m s^{-1} within 30 s before impacting the highway. We present a new technique to obtain high spatial and temporal resolution velocity estimates not previously demonstrated with infrasound for avalanches and other mass wasting events.

1. Introduction

Avalanche-generated infrasound was first detected on infrasound sensors deployed by the National Oceanic and Atmospheric Administration in Boulder, CO [*Bedard*, 1989, 1994; *Bedard et al.*,1988]. The authors found avalanches generate acoustic signals in the 1–5 Hz region and the work led others to develop infrasound systems focused on avalanche detection [*Chritin et al.*, 1996; *Scott et al.*, 2007; *Ulivieri et al.*, 2011]. Several systems are now used operationally by highway forecasters in the United States, which provides necessary information on avalanche activity to avalanche forecasters [*Yount et al.*, 2008].

One method previously demonstrated for tracking avalanches uses seismometers in the avalanche path and detects when the avalanche reaches each station [e.g., *Vilajosana et al.*, 2007]. Using the location of the seismometers and the time the avalanche moves over the seismometers, the velocity between stations can be calculated. *Lacroix et al.* [2012] deployed a seismometer array away from the avalanche path and used beam forming to calculate the velocity as a function of time. Typical avalanche velocities using seismic methods from previous studies are shown in Table 1. Avalanche velocities calculated using seismic methods show avalanche average velocities vary between 5 and 57 m s^{-1} for dry and wet avalanches.

Other techniques for tracking avalanche velocity include videogrammetry [*Vallet et al.*, 2004], arrays of pressure pylons placed directly in the avalanche path [*Kogelnig et al.*, 2011], or upward looking Frequency Modulated Continuous Wave (FMCW) radars [*Gubler and Hiller*, 1984]. A FMCW doppler radar placed at the base of the path [*Vriend et al.*, 2013] can calculate the avalanche velocity over time using feature tracking but is constrained to monitor only a single avalanche path and can be prohibitively expensive.

Other mass wasting events, like pyroclastic flows, have similar flow dynamics and behaviors to avalanches. *Ripepe et al.* [2009] tracked a pyroclastic flow with an infrasound array and first gave insight into calculating the velocity with infrasound. However, the authors only looked at the average velocity of the flow during the entire event. *Yamasato* [1997] tracked pyroclastic flows using both seismic and infrasound sensors deployed around the volcano. The velocity was estimated using the Doppler shift of the infrasound microphones.

Here we present an avalanche event that was recorded on a nearby infrasound array. Using array processing techniques and Monte Carlo simulations of probable source locations, we calculate the velocity with uncertainties for the avalanche.

Table 1. Avalanche Velocities Calculated Using Different Methods

Source	Avalanche Type	Method	Velocity (m s^{-1})
Kishimura and Izumi [1997]	Dry avalanches	Seismic	25–57
Lacroix et al. [2012]	Dry and wet avalanches	Seismic	12–32
Takeuchi et al. [2003]	Dry and wet avalanches	Seismic	20–43
Vilajosana et al. [2007]	Dry avalanches	Seismic	5–55
Caplan-Auerbach et al. [2004]	Ice avalanche from volcano, triggered by earthquakes	Seismic	14–70
van der Woerd et al. [2004]	Earthquake-triggered ice avalanche	Seismic	21–35
Huggel et al. [2007]	Large ice avalanches from volcano	Seismic	22–70
Vallet et al. [2004]	Dry avalanche	Videogrammetry	10–55
Kogelnig et al. [2011]	Dry and wet avalanches	Pressure pylons	20–55
Vriend et al. [2013]	Dry avalanches	FMCW radar	5–40

2. The 96.92 Avalanche Event

2.1. Avalanche Cycle

The avalanche cycle on 19 January 2012 proved to be one of the largest avalanche cycles that the Highway 21 corridor has ever experienced (Figure 1a). Two separate avalanche cycles occurred during the 7 day storm; the first avalanche cycle produced large dry avalanches, and the second avalanche cycle produces medium wet avalanches. In two and a half days leading to the first avalanche cycle, the storm produced 0.07 m of water and approximately 0.56 m of snow at a automated weather station (2180 m above sea level (asl)) 16 km to the north at Banner Summit.

After the storm cleared, the storm totals were 1.34 m of snow, 0.129 m of water, and 57 reported avalanches. Debris on the highway ranged from 1.5 to 8 m deep from 37 different avalanches. Figure 1a provides an overview of the highway corridor and the avalanche paths that were active during the avalanche cycle.

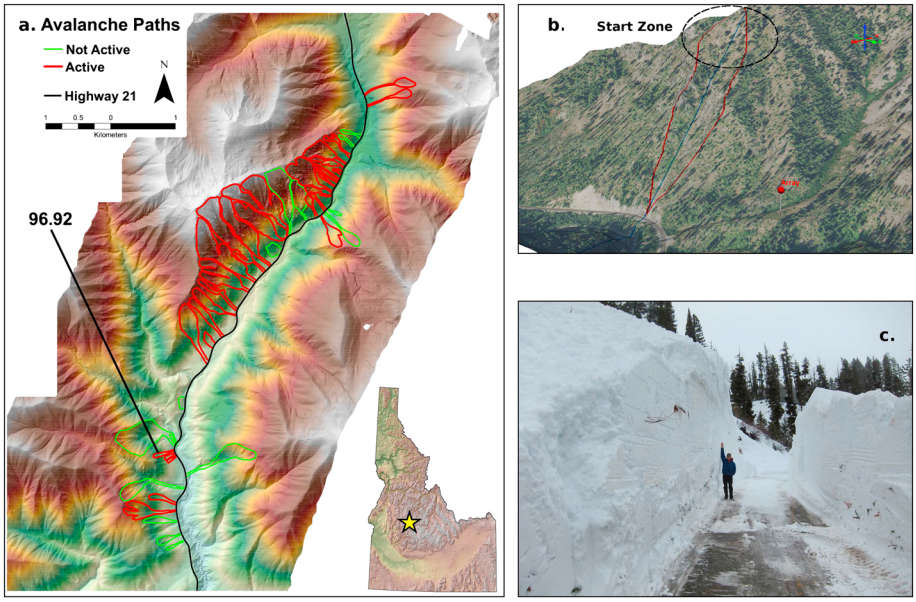

Figure 1. (a) Overview of Highway 21 through the Canyon Creek corridor in Central Idaho. A significant number of the major avalanche paths had evidence of extremely large dry avalanches which occurred during the 19 January 2012 cycle. A total of 57 avalanches were reported in the area, with 37 avalanches that covered the highway with 1.5 to 8 m of snow. (b) Three-dimensional rendering obtained from a 2 m aerial lidar survey, overlain with 0.5 m orthophoto. The maximum extent of 96.92 is outlined in red with the path profile in blue. The infrasound array was located at the red marker. (c) Head avalanche forecaster standing in the middle of the debris pile a day after the 96.92 avalanche event. The debris was approximately 8 m high on the highway and continued to flow into the creek below. The array location is on the small ridge directly behind the forecaster.

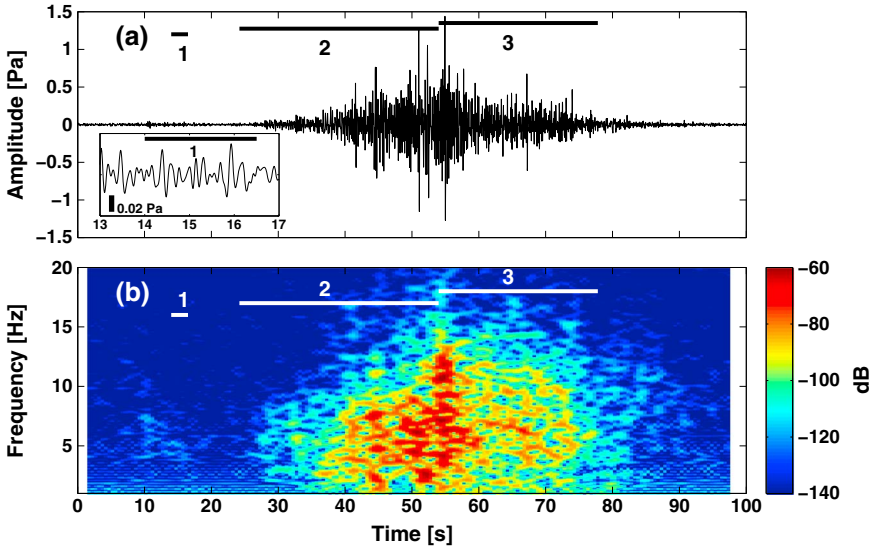

Figure 2. (a) Avalanche signal with the three phases marked. The highest amplitude of 1.5 Pa occurs when the avalanche reaches the highway. Inlay shows the whumpf signal with a two order of magnitude difference in amplitude. (b) Power spectrum of avalanche with the most power in the 1–10 Hz bandwidth. Higher frequencies appear after avalanche reaches the highway.

2.2. Path Characteristics

The 96.92 avalanche path is a small avalanche path with a high return interval (about 2.5 avalanches per year). The starting zone is relatively small, estimated to be 60 to 100 m wide, with a maximum elevation of 1970 m asl. The avalanche track (Figure 1b) is a maximum of 620 m in length, has an average slope of 31° with a maximum slope of 37°, and has a vertical drop of 370 m to the highway (1600 m asl). The path does not have a traditional run out zone where the avalanche can slowly lose momentum. Instead, the avalanche funnels through a 15 m channel immediately before reaching the highway (Figure 1c). Large events typically continue across the highway and into the creek below.

2.3. Avalanche Characteristics

The avalanche occurred on 19 January 2012 at 16:36 UTC and lasted approximately 64 s. The signal amplitude (Figure 2a) shows the classic infrasound signal characteristics of an avalanche with a gradually increasing ($t = 30$ s) amplitude as the avalanche gains momentum and size [*Kogelnig et al.*, 2011], then decreasing amplitude ($t = 60$ s) as the avalanche reaches the highway and stops. A maximum pressure of just under 1.5 Pa ($t = 55$ s) was recorded at a distance of approximately 300 m.

Prior to the avalanche at 14 s (Figure 2), there was a small precursory signal before the signal direction moves downslope. We hypothesize that the signal was from the snowpack fracture propagation which displaced the snowpack and caused the pressure wave in the air (i.e., a "whumpf") [*McClung and Schaerer*, 2006]. We believe that this is the first published example of a potential snowpack failure event captured remotely on an infrasound array. Snowpack failure has been observed during one opportunistic seismic study [*Johnson et al.*, 2004] but has not been recorded with infrasound.

The power spectrum (Figure 2b) of the avalanche indicates that most energy was in the 1–10 Hz bandwidth and agrees with previous work [e.g., *Bedard*, 1994; *Ulivieri et al.*, 2011]. High-frequency components were prevalent after the avalanche reached the highway.

3. Methods

3.1. Array Configuration

The array was located approximately 550 m away from the start zone and 270 m away from where the avalanche path intersects the highway. The back azimuth ranged from 216 (start zone) to 162° (highway), a 54° sweep, providing an ideal array placement for calculating velocity. The array consisted of three

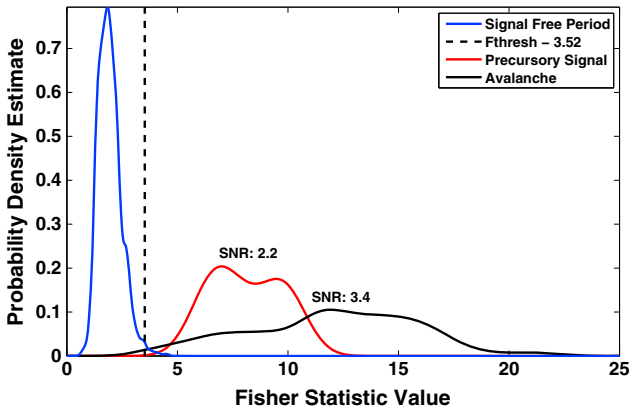

Figure 3. The probability density function (PDF) of the 10 min signal-free period, the precursory signal, and the avalanche are compared. The Fisher statistic threshold was the 0.99 quantile of the signal-free period. The median value of the signals over the threshold was the signal to noise ratio (SNR), with the precursory and avalanche signal well above the Fisher statistic threshold value.

infrasound sensors with a flat frequency response in the 1–20 Hz frequency band [*Marcillo et al.*, 2012] and 30 m spacing in a triangular arrangement. The sensors were recorded on a RefTek 130 at 100 Hz and 24 bit analog-to-digital converter.

3.2. Calculating the Fisher Statistic

The Fisher statistic [e.g., *Smart and Flinn*, 1971; *Blandford*, 1974] is a measure of signal coherence and is the power of the beam divided by the average difference in power of the beam and individual channels. The Fisher statistic assumes a single point source with perfectly correlated signal and perfectly uncorrelated noise [*Blandford*, 1974]. Following *Smart and Flinn* [1971], the Fisher statistic in the frequency domain is defined as

$$F(\omega, \mathbf{s}) = \frac{E(\omega, \mathbf{s})}{E(\omega) - E(\omega, \mathbf{s})} \cdot (N - 1) \tag{1}$$

where

$$E(\omega, \mathbf{s}) = \left| \frac{1}{N} \sum_{j=1}^{N} A_j(\omega) \cdot \exp(-i\omega \mathbf{s} \cdot \mathbf{r_j}) \right|^2 \tag{2}$$

and

$$E(\omega) = \frac{1}{N} \sum_{j=1}^{N} \left| A_j(\omega) \right|^2 \tag{3}$$

with N sensors located at position vectors $\mathbf{r_j}$, $A_j(\omega)$ contains the amplitude information from the Fourier transform and slowness $\mathbf{s}$.

The slowness vector $\mathbf{s}$ points from the array to the possible source location with the exponential in equation (2) applying the necessary time shifts for the array geometry given the source location. The slowness vector was calculated every 2 m horizontally along the path profile (Figure 4c), which was derived from a 2 m Digital Elevation Model. The speed of sound was calculated using an air temperature of −1.1°C (331 m s^{-1}) recorded by a nearby remote weather station. The Fisher statistic (equation (1)) was evaluated at each slowness vector $\mathbf{s}$ along the path. When the Fisher statistic is maximized, the slowness vector provides a direct estimate of the back azimuth and incidence angle to the potential source location.

The frequency wave number (fk) analysis [*Rost and Thomas*, 2002] determines the time shifts required and evaluates the Fisher statistic for varying slowness vectors. The fk analysis can be performed for a short moving window with a constant step size, but the window size must be large enough to capture the dominant frequency moving across the array. The fk analysis was performed with a 1–10 Hz band-passed signal for a moving window of 4 s, overlapped by 3.5 s. Therefore, all potential source locations are evaluated along the path for each overlapping time window.

A 10 min signal-free period just prior to the avalanche was used to evaluate the threshold value of the Fisher statistic. In the 1–10 Hz bandwidth, the Fisher statistics fell into the probability density function (PDF) shown in Figure 3 with a 0.99 quantile of 3.52. The quantile became the Fisher statistic threshold value to evaluate whether or not signal was present above the noise.

3.3. Calculating Velocity

Avalanches, similar to other mass wasting events like pyroclastic flows, are a complex moving source believed to produce the majority of infrasound near the front of the flow [*Yamasato*, 1997]. To determine

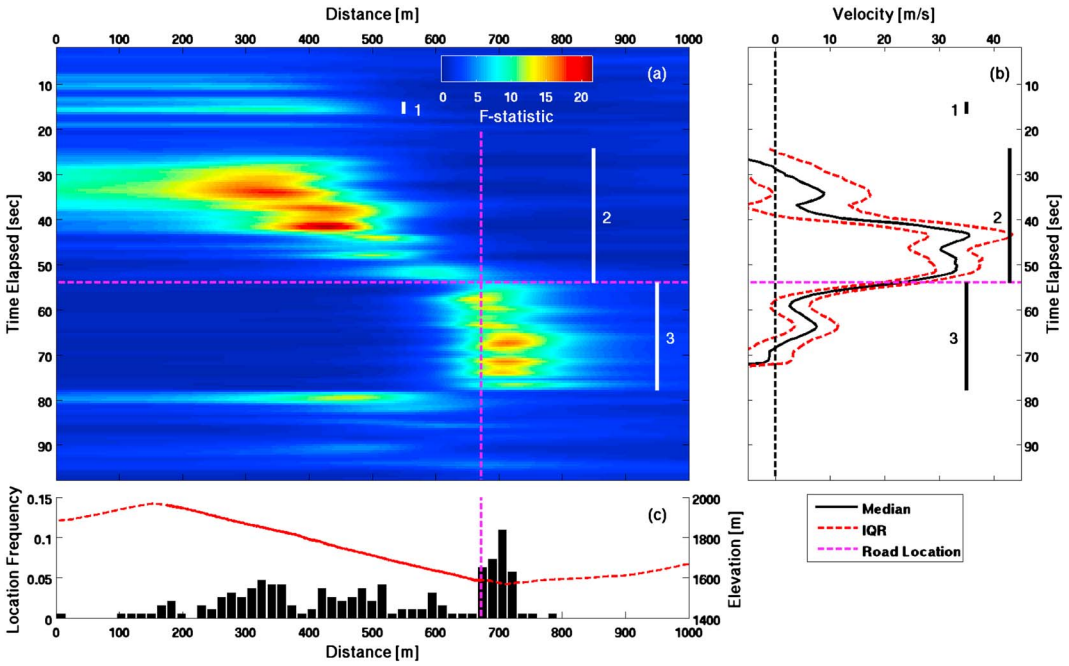

Figure 4. (a) F statistic evaluated at each point along the path profile in the 1–10 Hz bandwidth. The three avalanche phases are shown with the highway location highlighted. (b) Velocity of avalanche was slow to start but reaches a maximum of 35.9 ± 7.6 m s^{-1} just before reaching the highway. (c) The 96.92 path profile in red with a histogram of the maximum F statistic locations through time. The solid red shows the maximum extent of the 96.92 avalanche path with the snowpack failure and avalanche motion originating around 300–320 m.

the most probable source location of the avalanche, the Fisher statistic was calculated as a function of position along the avalanche path (Figure 4c). High Fisher statistic values represent a higher probability of the source location, similar to a PDF. The higher the probability density (or Fisher statistic value) the more likely the source came from that particular location along the avalanche path.

The estimated source location as a function of time was determined by randomly sampling the probable source locations based on the Fisher statistic probability at each time step. Therefore, a higher Fisher statistic has a higher probability of being randomly chosen. To reduce the large location jumps due to random sampling, the locations are smoothed with a 12 s Gaussian kernel. The velocity is the derivative downslope with a 2 m horizontal distance and 0.5 s time interval. One thousand Monte Carlo simulations were performed to determine the median and interquartile range of the velocity. This provides an estimate of the velocity and uncertainty as a function of time for the 64 s event.

4. Results and Discussion

4.1. The Three Avalanche Phases

The avalanche can be described in three different phases: the initial failure, acceleration in the track, and impact with the highway (Figure 4).

4.1.1. First Phase

The first phase was a small signal originating from the start zone at 10 s and lasting approximately 2.5 s. The signal has a peak amplitude of 0.035 Pa with the majority of the energy in the 4–9 Hz bandwidth. The signal was well above the background level of the Fisher statistic during the signal-free period (Figure 3) with a signal to noise ratio (SNR) of 2.2. This indicates a significant signal originated from the avalanche start zone (Figure 4a) just prior to the avalanche.

We interpret the precursory signal as the fracture initiation and propagation of the snowpack. *Johnson et al.* [2004] measured a propagating failure using a string of geophones on the snow surface in a flat meadow. The fracture propagated away from the trigger point at 20 m s^{-1} from a compressive fracture that created a bending wave in the overlaying slab due to the sudden vertical movement. Similar fracture

propagation velocities of 27 to 36 m s^{-1} have been observed in snow stability tests recorded with high-speed video [*van Herwijnen et al.*, 2010]. *Bair et al.* [2012] used high-speed video to estimate the vertical displacement of the slab and measured 1–2 mm of vertical movement in storm snow . The vertical slab movement induces a vibration in the atmosphere just above the slab, causing the whumpf sound [*Schweizer et al.*, 2003].

The precursory signal has a small amplitude which is consistent for a small vertical displacement of the slab (Figure 2a). If the fracture propagated across the entire start zone of 60 m over a measured 2.5 s, the average propagation velocity would be 24 m s^{-1} which agrees with values observed by *van Herwijnen et al.* [2010].

4.1.2. Second Phase

The second phase starts at 24.2 s with the first detectable signal from the avalanche and lasts until the avalanche reaches the highway at 54.0 s (Figure 4a). The time delay between the first and second phase could be due to the time needed for the failure to propagate across the slope and for the avalanche to reach the minimum momentum to generate detectable infrasound caused by atmospheric displacement [*Kogelnig et al.*, 2011]. Between the first and second phases, the Fisher statistic ranges between 2.0 and 3.5, which was below the threshold. This indicates that there was no significant signal detected.

As an avalanche moves down the path, a suspension layer forms at a velocity of approximately 10 m s^{-1} [*McClung and Schaerer*, 2006] due to the turbulent eddies caused by the friction between the avalanche and atmosphere. We believe a suspension layer formed sometime between 24.2 and 43.3 s as the avalanche gained momentum. Once the suspension layer formed, the avalanche quickly accelerated to the maximum velocity of 35.9 ± 7.6 m s^{-1} approximately 300 m from the highway (43.3 s). A small decrease in velocity can be seen in Figure 4b before increasing to 33.5 ± 4.2 m s^{-1} at 48.8 s right before impact with the highway. Our velocity observations are smoothed in space and time and this therefore provides a lower-bound estimate of the velocity.

4.1.3. Third Phase

The third phase occurs after the avalanche impacts the highway at 54.0 s. The infrasound signal recorded comes from a constant location at the intersection of the avalanche path and highway, as the avalanche continues to deposit snow on the highway and overflows into the creek for 23.8 s.

4.2. Avalanche Velocity

The average velocity of the avalanche was 14.5 m s^{-1} from the first major signal at 24.2 s to the impact with the highway at 54.0 s and was in the lower range of previous observations (Table 1). The average velocity was of reasonable magnitude but is highly path dependent as the avalanche did not likely have enough time to reach a steady terminal velocity and was possibly still accelerating when it impacted the highway.

The measured avalanche velocity can be described by the velocity of a mass-gaining momentum as it moves down slope (Figure 4b). Initially, the velocity was small as the initial snow mass began to move. As the avalanche gained momentum, a suspension layer likely formed and produced a high-amplitude infrasound signal [*Kogelnig et al.*, 2011] with high Fisher statistic values. The avalanche accelerated quickly to a maximum velocity of 35.9 ± 7.6 m s^{-1} within approximately 300 m of the highway as more snow was entrained right before it impacted the highway.

5. Conclusions

For the first time, the velocity time series of an avalanche was tracked from beginning to end using an infrasound array with optimal placement. Most seismic studies of avalanches have only been able to determine the average avalanche velocity, with a few studies calculating velocity time series for a specific path from radar (Table 1). The average velocity we calculated (14.5 m s^{-1}) was significantly less than the estimated maximum velocity of 35.9 ± 7.6 m s^{-1} and was in the lower range of previous observations, likely due to the relatively short avalanche path.

The large avalanche had three distinct phases. The avalanche started with the failure of the weak layer 10 s prior to the first detectable signal of the avalanche. We believe this to be the first time a possible weak layer failure has been captured using infrasound. Having the array 550 m from the start zone allowed for the detection of the small amplitude signal. Once the avalanche gained momentum, it quickly accelerated

downslope to a maximum velocity of 35.9 ± 7.6 m s^{-1} before impacting the highway. After the avalanche front impacted the highway, it takes 23.8 s for the remaining mass of the avalanche to lose momentum as it reached the highway and filled the creek below.

The technique presented is promising for estimating the velocity of a moving source when the infrasound array is ideally located close to the avalanche path with a large change in back azimuth. However, the technique may not apply to events further away from the array as there may not be the necessary back azimuth range needed to calculate a high-resolution velocity estimate.

In the future, infrasound combined with video and time lapse photography will help determine the sources of infrasound generated by the avalanche. The measured air pressure and velocity estimates, combined with an avalanche dynamics modeling, could allow infrasound estimates of the volume and mass of snow deposited on the highway, which would be useful for estimating highway cleanup requirements for multiday closures.

Acknowledgments

The authors would like to thank the avalanche forecasters at Idaho Transportation Department for the weather and avalanche data. Support for this research was provided by Idaho Transportation Department research project RP219, NASA grant 12-EARTH12R-49 (NASA Earth and Space Sciences Fellowship), NSF EAR grant 1151662, and IRIS PASSCAL. The avalanche infrasound data can be obtained by contacting the corresponding author directly. Two anonymous reviewers provided valuable comments that improved this manuscript.

The Editor thanks Emanuele Marchetti and an anonymous reviewer for their assistance in evaluating this paper.

References

Bair, E. H., R. Simenhois, K. Birkeland, and J. Dozier (2012), A field study on failure of storm snow slab avalanches, *Cold Reg. Sci. Technol.*, *79-80*, 20–28, doi:10.1016/j.coldregions.2012.02.007.

Bedard, A. J., Jr. (1989), Detection of avalanches using atmospheric infrasound, in *Proceedings of Western Snow Conference,* edited by B. Shafer, pp. 52–58, Colorado State Univ., Fort Collins, Colo.

Bedard, A. J., Jr. (1994), An evaluation of atmospheric infrasound for monitoring avalanche, in *Proceedings of 7th International Symposium on Acoustic Sensing and Associated Techniques of the Atmosphere and Oceans*, NOAA/ERL/Environmental Technology Laboratory, Boulder, Colo.

Bedard, A. J., Jr., G. E. Greene, J. Intrieri, and R. Rodriguez (1988), On the feasibility and value of detecting and characterizing avalanches remotely by monitoring radiated sub-audible atmospheric sound at long distances, in *Proceedings of A Multidisciplinary Approach to Snow Engineering*, pp. 267–275, U.S. Army Corps of Engineers, Cold Regions Research and Engineering Laboratory, Santa Barbara, Calif.

Blandford, R. R. (1974), An automatic event detector at the Tonto forest seismic observatory, *Geophysics*, *39*(5), 633–643.

Caplan-Auerbach, J., S. Prejean, and J. Power (2004), Seismic recordings of ice and debris avalanches on Iliamna volcano (Alaska), *Acta Vulcanologica*, *16*(1–2), 9–20.

Chritin, V., M. Rossi, and R. Bolognesi (1996), Acoustic detection system for operational avalanche forecasting, in *Proceedings of the 1996 International Snow Science Workshop,* pp. 129–133, Banff, Alta., Canada.

Gubler, H., and M. Hiller (1984), The use of microwave FMCW radar in snow and avalanche research, *Cold Reg. Sci. Technol.*, *9*, 109–119.

Huggel, C., J. Caplan-Auerbach, C. F. Waythomas, and R. L. Wessels (2007), Monitoring and modeling ice-rock avalanches from ice-capped volcanoes: A case study of frequent large avalanches on Iliamna Volcano Alaska, *J. Volcanol. Geotherm. Res.*, *168*(1–4), 114–136, doi:10.1016/j.jvolgeores.2007.09.009.

Johnson, B., J. Jamieson, and R. Stewart (2004), Seismic measurement of fracture speed in a weak snowpack layer, *Cold Reg. Sci. Technol.*, *40*(1–2), 41–45, doi:10.1016/j.coldregions.2004.05.003.

Kishimura, K., and K. Izumi (1997), Seismic signals induced by snow avalanche flow, *Nat. Hazard.*, *15*(1), 89–100, doi:10.1023/A:1007934815584.

Kogelnig, A., E. Surinach, I. Vilajosana, J. Huebl, B. Sovilla, M. Hiller, and F. Dufour (2011), On the complementariness of infrasound and seismic sensors for monitoring snow avalanches, *Nat. Hazards Earth Syst. Sci.*, *11*(8), 2355–2370, doi:10.5194/nhess-11-2355-2011.

Lacroix, P., J. R. Grasso, J. Roulle, G. Giraud, D. Goetz, S. Morin, and A. Helmstetter (2012), Monitoring of snow avalanches using a seismic array: Location, speed estimation, and relationships to meteorological variables, *J. Geophys. Res.*, *117*, F01034, doi:10.1029/2011JF002106.

Marcillo, O., J. B. Johnson, and D. Hart (2012), Implementation, characterization, and evaluation of an inexpensive low-power low-noise infrasound sensor based on a micromachined differential pressure transducer and a mechanical filter, *J. Atmos. Oceanic Technol.*, *29*(9), 1275–1284, doi:10.1175/JTECH-D-11-00101.1.

McClung, D. M., and P. Schaerer (2006), *The Avalanche Handbook*, The Mountaineers, Seattle, Wash.

Ripepe, M., S. DeAngelis, G. Lacanna, P. Poggi, C. Williams, E. Marchetti, D. D. Donne, and G. Ulivieri (2009), Tracking pyroclastic flows at Soufrière Hills Volcano, *Eos Trans. AGU*, *90*, 229–236.

Rost, S., and C. Thomas (2002), Array seismology: Methods and applications, *Rev. Geophys.*, *40*(3), 1008, doi:10.1029/2000RG000100.

Schweizer, J., J. Jamieson, and M. Schneebeli (2003), Snow avalanche formation, *Rev. Geophys.*, *41*(4), 1016, doi:10.1029/2002RG000123.

Scott, E. D., C. T. Hayward, R. F. Kubichek, J. C. Hamann, J. W. Pierre, B. Comey, and T. Mendenhall (2007), Single and multiple sensor identification of avalanche-generated infrasound, *Cold Reg. Sci. Technol.*, *47*(1–2), 159–170, doi:10.1016/j.coldregions.2006.08.005.

Smart, E., and E. A. Flinn (1971), Fast frequency-wavenumber analysis and fisher signal detection in real-time infrasonic array data processing, *Geophys. J. Int.*, *26*(1–4), 279–284, doi:10.1111/j.1365-246X.1971.tb03401.x.

Takeuchi, Y., K. Yamanoi, Y. Endo, S. Murakami, and K. Izumi (2003), Velocities for the dry and wet snow avalanches at Makunosawa valley in Myoko, Japan, *Cold Reg. Sci. Technol.*, *37*(3), 483–486, doi:101016/S0165-232X(03)00086-7.

Ulivieri, G., E. Marchetti, M. Ripepe, I. Chiambretti, G. De Rosa, and V. Segor (2011), Monitoring snow avalanches in Northwestern Italian Alps using an infrasound array, *Cold Reg. Sci. Technol.*, *69*(2–3), 177–183, doi:10.1016/j.coldregions.2011.09.006.

Vallet, J., B. Turnbull, S. Joly, and F. Dufour (2004), Observations on powder snow avalanches using videogrammetry, *Cold Reg. Sci. Technol.*, *39*(2–3), 153–159, doi:10.1016/j.coldregions.2004.05.004.

van der Woerd, J., L. Owen, P. Tapponnier, X. Xu, F. Kervyn, R. Finkel, and P. Barnard (2004), Giant, similar to M8 earthquake-triggered ice avalanches in the Eastern Kunlun Shan, Northern Tibet: Characteristics, nature and dynamics, *Geol. Soc. Am. Bull.*, *116*(3–4), 394–406, doi:10.1130/B25317.1.

van Herwijnen, A., J. Schweizer, and J. Heierli (2010), Measurement of the deformation field associated with fracture propagation in weak snowpack layers, *J. Geophys. Res.*, *115*, F03042, doi:10.1029/2009JF001515.

Vilajosana, I., G. Khazaradze, E. Surinach, E. Lied, and K. Kristensen (2007), Snow avalanche speed determination using seismic methods, *Cold Reg. Sci. Technol.*, *49*(1), 2–10, doi:10.1016/j.coldregions.2006.09.007.

Vriend, N. M., J. N. McElwaine, B. Sovilla, C. J. Keylock, M. Ash, and P. V. Brennan (2013), High-resolution radar measurements of snow avalanches, *Geophys. Res. Lett.*, *40*(4), 727–731, doi:10.1002/grl.50134.

Yamasato, H. (1997), Quantitative analysis of pyroclastic flows using infrasonic and seismic data at Unzen Volcano, Japan, *J. Phys. Earth*, *45*, 397–416.

Yount, J., A. Naisbitt, and E. D. Scott (2008), Operational highway avalanche forecasting using the infrasonic avalanche detection system, in *International Snow Science Workshop Proceedings, Whistler, BC*, pp. 265–276.